COBEM UBERLÂNDIA 2019

ABCM Associação Brasileira de Engenharia e Ciências Mecânicas

25th ABCM International Congress of Mechanical Engineering
October 20-25, 2019, Uberlândia, MG, Brazil

COB-2019-0520
COMPARATIVE STUDY THROUGH BOUNDARY ELEMENT ANALYSIS OF KIRCHHOFF PLATES

Carlos Lamarca Carvalho Sousa Esteves
Carlos Henrique Daros
Department of Computational Mechanics, Faculty of Mechanical Engineering, State University of Campinas, 200 Mendeleyev Street, 13083-860, Campinas, SP, Brazil
carloslamarcaesteves@outlook.com
chdaros@fem.unicamp.br

Abstract. *This paper aims to study the difference in the usage of methodologies when analyzing Kirchhoff's plate bending problem under three different models using the boundary element method: quadratic continuous elements using both plate's displacement and rotation equations; quadratic continuous elements using only displacement equation with points outside the boundary; quadratic discontinuous elements. The Shift Point Method was also integrated for evaluation of the Hadamard finite part when treating the hypersingular term from the rotation equation. The curvature of the element was taken into consideration in order to properly analyze curved plates. Conversion of the domain integral regarding acting body forces into a boundary integral was also implemented for speed. The first model showed better results overall in convergence and consistency of the results under different plate shapes and boundary conditions.*

Keywords: *Kirchhoff plate, Boundary Element, Corners*

1. INTRODUCTION

Many are the engineering problems that are more easily solved through approximation rather than obtaining the analytical value. A classical example for this are the plates used in naval and aerospace engineering. One of the ways to solve the plate bending problem is to use the Boundary Element Method as it was published by Brebbia and Dominguez (1991). Starting from this simple application in elastostatic, many authors followed on developing the method further. Stern (1979) published the Boundary Integral formulation for plates with non-smooth boundaries proposing the much needed fundamental solutions and evaluating the free terms. Hartmann and Zotemantel (1986) then focuses on the numerical treatment of integrals using linear elements and detailing the evaluation of Cauchy principal values. Then, Venturini and Paiva (1993) compiles different methodologies and compare their results for rectangular plates. More recently, Katsikadelis (2014) presents in detail the formulation for the various applications of BEM in plate bending that have been developed throught history.

In this paper, three methodologies to assess the Boundary Integral Equation for Kirchhoff's plates will be explored: the continuous model, the outside points' model and the discontinuous model. The continuous model consists of continuous quadratic curved elements using both displacement and rotation equations where nodes will be shifted (Shifted Point Method) when using the rotation equation. The outside model consists of continuous quadratic curved elements using only the displacement equation with points outside the boundary (half of the element size in distance) to complete the number of equations required. The discontinuous model consists of discontinuous quadratic curved elements using both displacement and rotation equations. All of them were subjected to a uniformly distributed load which was evaluated using radial integration as formulated by Gao (2002).

2. PLATE BOUNDARY INTEGRAL FORMULATION

As noted from Venturini and Paiva (1993), the isotropic displacement integral equation for Kirchhoff's plate bending theory is fairly well known and used. However, even this simple isotropic problem can be studied in different ways depending on the approach used regarding geometry, node placement and shape functions. It is shown in Eq. (1) the integral formulation for plate bending under a transverse load:

$$c_i(\xi)w(\xi) + \int_\Gamma [V_n^*(\xi,\mathbf{x})w(\mathbf{x}) - M_n^*(\xi,\mathbf{x})\frac{\partial w}{\partial n}(\mathbf{x})]d\Gamma + \sum_{j=1}^{N_c} R_j^*(\xi,j)w_{c_j}(\mathbf{x}) =$$
$$\int_\Gamma [w^*(\xi,\mathbf{x})V_n(\mathbf{x}) - \left(\frac{\partial w}{\partial n}\right)^*(\xi,\mathbf{x})M_n(\mathbf{x})]d\Gamma + \sum_{j=1}^{N_c} R_j(\xi,j)w_j^*(\mathbf{x}) + \int_\Omega b(\mathbf{x})w^*(\xi,\mathbf{x})d\Omega, \quad (1)$$

$$c_i(\xi)\frac{\partial w}{\partial n_i}(\xi) + \int_\Gamma \left[\left(\frac{\partial V_n}{\partial n_i}\right)^*(\xi,\mathbf{x})w(\mathbf{x}) - \left(\frac{\partial M_n}{\partial n_i}\right)^*(\xi,\mathbf{x})\frac{\partial w}{\partial n}(\mathbf{x})\right]d\Gamma + \sum_{j=1}^{N_c}\left(\frac{\partial R_j}{\partial n_i}\right)^*(\xi,j)w_{c_j}(\mathbf{x}) =$$
$$\int_\Gamma \left[\left(\frac{\partial w}{\partial n_i}\right)^*(\xi,\mathbf{x})V_n(\mathbf{x}) - \left(\frac{\partial^2 w}{\partial n_i \partial n}\right)^*(\xi,\mathbf{x})M_n(\mathbf{x})\right]d\Gamma + \sum_{j=1}^{N_c} R_j(\xi,j)\left(\frac{\partial w_j}{\partial n_i}\right)^*(\mathbf{x}) + \int_\Omega b(\mathbf{x})\left(\frac{\partial w}{\partial n_i}\right)^*(\xi,\mathbf{x})d\Omega, \quad (2)$$

where $c_i(\xi)$ is the free term of the source point, V_n^*, M_n^*, w^*, $(\frac{\partial w}{\partial n})^*$ and R_j^* are the fundamental solutions for the effective shear force, bending, displacement, rotation and corner reaction respectively. But Eq. (1) doesn't provide enough equations to solve the problem. This can be fixed with either using point collocation outside of the boundary or by deriving Eq. (1) in a specific direction (similarly done in Venturini and Paiva (1993) and Tanaka and Bercin (1998)). For the purpose of this paper, it was derived in relation to the outwards normal of the source point (n_i), as showed in Eq. (2). A generic plate problem that can be analysed using the models in this paper is represented in Fig. 1 as it is under the uniformly distributed load $b(\mathbf{x})$, clamped on one side (**C**), simply supported (**S**) on another and two free (**F**) curved boundaries that meet at the free corner with displacement of w_c.

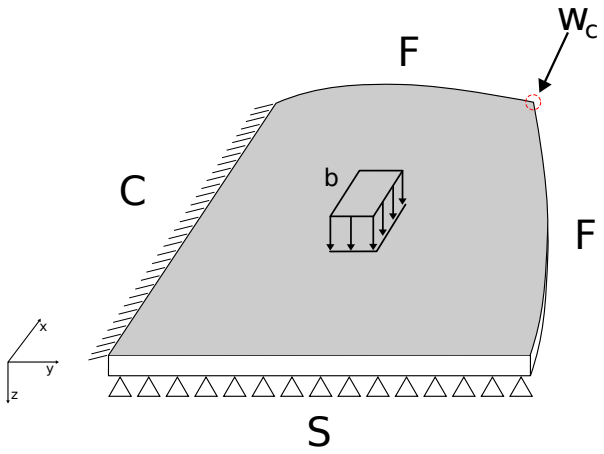

Figure 1. Generic plate model

In order to solve the problem with Eq. (1) and Eq. (2), boundary discretization will follow for a number of quadratic elements. In matrix terms:

$$\mathbf{H}_V\mathbf{w} - \mathbf{H}_M\frac{\partial \mathbf{w}}{\partial \mathbf{n}} + \mathbf{R}_1\mathbf{w}_c = \mathbf{G}_w\mathbf{V}_n - \mathbf{G}_\theta\mathbf{M}_n + \mathbf{C}_1\mathbf{R}_c + \mathbf{b}_1, \quad (3)$$

$$\mathbf{H}_{V_i}\mathbf{w} - \mathbf{H}_{M_i}\frac{\partial \mathbf{w}}{\partial \mathbf{n}} + \mathbf{R}_2\mathbf{w}_c = \mathbf{G}_{w_i}\mathbf{V}_n - \mathbf{G}_{\theta_i}\mathbf{M}_n + \mathbf{C}_2\mathbf{R}_c + \mathbf{b}_2. \quad (4)$$

Both Eq. (3) and Eq. (4) can be joined to form a single system of equations as follows in Eq. (5):

$$\begin{bmatrix}\mathbf{H}_V & -\mathbf{H}_M \\ \mathbf{H}_{V_i} & -\mathbf{H}_{M_i}\end{bmatrix}\begin{bmatrix}\mathbf{w} \\ \frac{\partial \mathbf{w}}{\partial \mathbf{n}}\end{bmatrix} + \begin{bmatrix}\mathbf{R}_1 \\ \mathbf{R}_2\end{bmatrix}\mathbf{w}_c = \begin{bmatrix}\mathbf{G}_w & -\mathbf{G}_\theta \\ \mathbf{G}_{w_i} & -\mathbf{G}_{\theta_i}\end{bmatrix}\begin{bmatrix}\mathbf{V}_n \\ \mathbf{M}_n\end{bmatrix} + \begin{bmatrix}\mathbf{C}_1 \\ \mathbf{C}_2\end{bmatrix}\mathbf{R}_c + \begin{bmatrix}\mathbf{b}_1 \\ \mathbf{b}_2\end{bmatrix},$$
$$\mathbf{H}\,\mathbf{u} + \mathbf{R}\mathbf{w}_c = \mathbf{G}\mathbf{q} + \mathbf{C}\mathbf{R}_c + \mathbf{b}. \quad (5)$$

where $\mathbf{u}$ is the vector containing the displacements and the rotations, $\mathbf{q}$ is the vector containing the effective shear and bending moments, $\mathbf{H}$ is the matrix with the influence values relative to $\mathbf{u}$ from both equations, $\mathbf{G}$ is the matrix with the influence values relative to $\mathbf{q}$ from both equations, $\mathbf{w}_c$ and $\mathbf{R}_c$ are the displacements and the reactions at the corners with $\mathbf{R}$ and $\mathbf{C}$ being their respective influence matrices and $\mathbf{b}$ is the vector corresponding to the acting body forces.

After applying the boundary conditions, Eq. (5) can be turned in the linear system of Eq. (6):

$$[\mathbf{A}]\{x\} = \{p\} + \{b\}, \tag{6}$$

where $\{p\}$ is the product of the known variables and the resulting matrix after boundary conditions are applied. Since this work won't analyze situations with loads on the boundary, $\{p\}$ is always zero.

3. METHODOLOGY

In this section, it will be discussed the considerations made when using each of the three models proposed for comparison. For all three, the curvature of the element was taken into consideration, adding a new term in V_n^* and its derivative and thus allowing the possibility of analyzing curved plates with more fidelity to the original geometry. Since the shape functions were used to parameterize the geometry for the non-dimensional variable ξ, the curvature function was evaluated as described in Eq. (7) (the second derivative exists and can be different from zero as the shape functions are of second order):

$$\frac{1}{\rho} = \frac{(x'(\xi)^2 + y'(\xi)^2)^{3/2}}{|x'(\xi)y''(\xi) - y'(\xi)x''(\xi)|}, \tag{7}$$

where $x(\xi)$ and $y(\xi)$ behave in each element with the shape functions in Eq. (8):

$$\begin{aligned} &\phi_1(\xi) = 0.5\xi(\xi - 1), \quad \phi_2(\xi) = 1 - \xi^2, \quad \phi_3(\xi) = 0.5\xi(1 + \xi), \\ &x(\xi) = x_1\phi_1(\xi) + x_2\phi_2(\xi) + x_3\phi_3(\xi), \\ &y(\xi) = y_1\phi_1(\xi) + y_2\phi_2(\xi) + y_3\phi_3(\xi). \end{aligned} \tag{8}$$

With that, just as detailed in Hartmann and Zotemantel (1986), the fundamental solutions will be as follows in Eq. (9):

$$\begin{aligned} &w^* = \frac{r^2 \ln r}{8\pi D}, \quad \frac{\partial w^*}{\partial n} = \frac{\partial r}{\partial n}\frac{(2r\ln r + r)}{8\pi D}, \quad M_n^* = -\frac{(1+\nu)(1+\ln r)}{4\pi} - \frac{(1-\nu)[2(\partial r/\partial n)^2 - 1]}{8\pi}, \\ &V_n^* = -\frac{\partial r}{\partial n}\frac{1}{4\pi r}\{2 + (1+\nu)[2(\partial r/\partial n)^2 - 1]\} + \frac{(1-\nu)\rho}{4\pi}[2(\partial r/\partial n)^2 - 1], \end{aligned} \tag{9}$$

where the radius (r) and flexural rigidity (D) are described in Eq. (10)

$$r = \sqrt{(x(\xi) - x_0)^2 + (y(\xi) - y_0)^2} \quad \text{and} \quad D = \frac{E\,h^3}{12(1-\nu^2)}. \tag{10}$$

A representation of the distance between any given field and source nodes with their respective normals are given in Fig. 2.

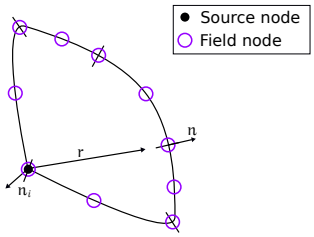

Figure 2. Element representation

For the quadratic continuous elements, it's important to take in consideration the continuity of the vertical displacement at each node connecting any two elements. The continuity of the other variables is also taken into consideration when needed (smooth connection). Since source nodes will be placed on the corners, the matrix $\mathbf{R}$ will be added to the respective columns of $\mathbf{H}_1$ (from Eq. (5)) as all w_c will now be equal to the displacement of some source nodes. In order to properly solve the problem using both equations, two separate sets of source points were created. Consider e.g. a fully campled triangular plate composed of three quadratic elements with 21 unknowns, Fig. 3 shows the distribution of required nodes for both sets of equations.

Set 1 was used for Eq. (1) and Set 2 for Eq. (2). For Set 1, data from the geometry were copied with additional situational points located near existing special nodes. Nodes were deemed special if boundary conditions changed discontinuously or if they were corner nodes. The number of extra nodes added was relative to the number of equations needed to solve the problem (which could change for the same geometry and mesh if different boundary conditions were

applied). These extra nodes do not add more variables to the problem since they will be located in existing elements (at either ξ = 2/3 or ξ = -2/3), therefore, values on that specific location can be interpolated from the existing variables of the element it belongs. This way, more equations can be added without increasing the number of unknown variables.

For Set 2, through the Shift Point Method, nodes connecting any two elements were shifted from ξ = -1 to ξ = -2/3 and ξ = 1 to ξ = 2/3. This was made in order to evaluate the Hadamard finite part for the hypersingular term, as the finite part is not defined at the ends of the element. Therefore, continuous shape functions were used with source nodes shifted from their original position. Additional nodes were also added to Set 2, according to necessity of the total of unknowns.

A pattern of point shifting was established: if the number of total elements was even, a 3-1-3 scheme was used; if the number of total elements was odd, a 3-1-2 scheme was used. The scheme refers to the positioning of the shifted nodes throughout the boundary elements. Figure 3 represents a simple model of a triangular plate with 3 elements following this directive for the case when all three sides are clamped. As all displacement and rotation are known to be zero, the three R_c, the nine V_n and the nine M_n sum up for a total of 21 unknowns (especial nodes 1, 3 and 5 have an extra V_n and M_n).

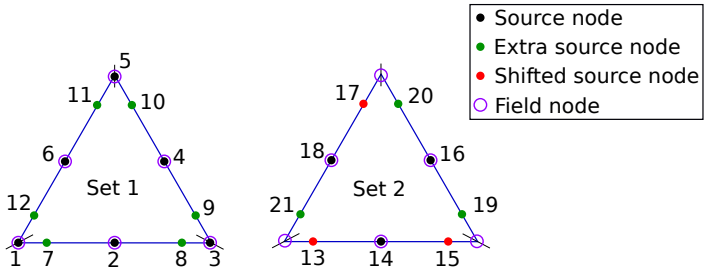

Figure 3. Representation of nodes - Continuous model

For the quadratic discontinuous elements, no reorganization in the matrices will follow since all variables were considered discontinuous. However, additional points were added in the corners to generate enough equations to solve the problem. Unlike the previous case, the number of extra equations was always equal to the number of special nodes in the problem. Since analytical solutions were specific to a certain position and sometimes the source node didn't land on said location, the value was obtained via extrapolation. It can be seen in Fig. 4 that all source nodes from the discontinuous model are located on the same locations as Fig. 3, but were generated from different mathematical considerations.

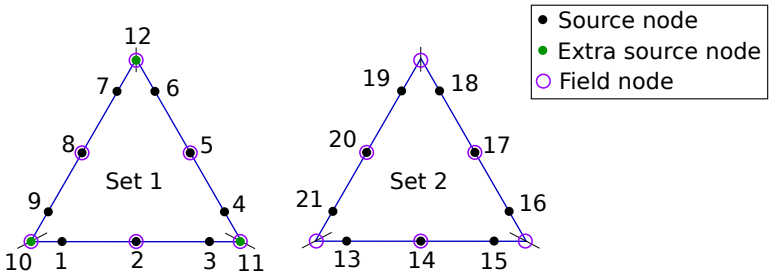

Figure 4. Representation of nodes - Discontinuous model

For the quadratic continuous elements with points outside, the same consideration for vertical displacement was made. What differs is that Set 1 can have additional nodes near special nodes and will be evaluated on Eq. (1). Placing nodes outside took into consideration half of the element size and the normal direction of the node. Corner nodes were considered to have 3 directions: one slightly before the node, one slightly after and one that was the vector sum of the other two directions. The number of extra equations needed might change depending on the boundary conditions applied.

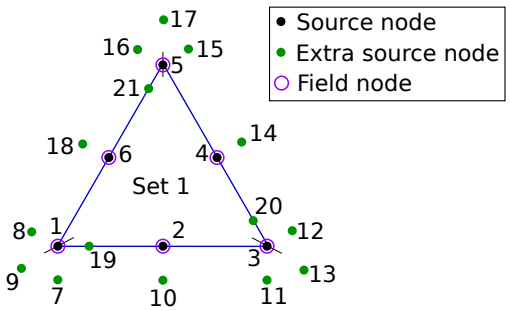

Figure 5. Representation of nodes - Outside points model

As each case was analyzed, it was observed that despite the low error displayed in the displacement data, the other variables presented highly divergent results (over 1000% in some cases). Not only that, as the inner angle of a corner increases (towards a smooth connection) both normals will tend to equality in direction. This resulted in three nodes numerically identical (as seen in Fig. 6), which in turn renders matrix $\mathbf{A}$ to be nearly singular or at least badly scaled (as all three points will generate nearly identical lines). To avoid this issue, and regarding the notation in Fig. 6, node 1 was made closer to the boundary (25% of the element size), node 2 was made further (100% of the element size) and node 3 kept its position (50% of the element size). This also allows the analysis of smooth surfaces with different boundary conditions.

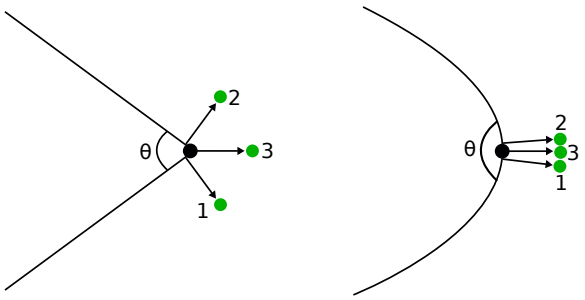

Figure 6. Transition as $\theta \to \pi$ rad

A secondary checkpoint to check the validity of the results was created by evaluating the integral of V_n over the boundary and summing this to the total R_c obtained had to equal the total body force acting on the plate, as equated in Eq. (11). This is a requirement since it's a static problem.

$$\int_{\Omega} \mathbf{b} d\Omega = \int_{\Gamma} \mathbf{V}_n d\Gamma + \sum_{j=1}^{N_c} \mathbf{R}_c. \tag{11}$$

Reference data and results from the algorithm were all normalized according to the formulas in Eq. (12):

$$\hat{w} = \frac{w\, D}{q_o\, L_r^4}, \qquad \hat{V_n} = \frac{V_n}{q_o\, L_r}, \qquad \hat{M_n} = \frac{M_n}{q_o\, L_r^2}, \tag{12}$$

where L_r is the reference dimension of the plate geometry. For the squared plate it's the size of either side; for the circle it's the radius; for the ellipse it's the small axis; for the extra example it's the horizontal side size.

A set of boundary conditions was chosen and ran through all three models with an increasing number of elements per "side". For each iteration, dimensionless data was extracted and it was taken the absolute relative difference from the reference value which was the analytical solution (as calculated by Timoshenko and Woinowsky-Krieger (1959) or Guminiak (2010)).

3.1 Boundary integral

Quadratic continuous nodal shape functions have been used to describe the geometry in all models and w, $\frac{\partial w}{\partial n}$, V_n and M_n in the continuous and the outside model while discontinuous functions were used for these variables in the discontinuous model. All of the regular integrals were evaluated using the standard Gaussian quadrature in the intrinsic variable ξ. Most of the integrals were regular, but singularities arise in the integrals regarding M_n^* (in $\mathbf{H}_M$), $(\frac{\partial^2 w}{\partial n_i \partial n})^*$ (in $\mathbf{G}_{w_i}$) and $(\frac{\partial V_n}{\partial n_i})^*$ (in $\mathbf{H}_{V_i}$). While the first two are weakly singular, the latter is hyper singular. The weak singular integrals were split into a regular term and a singular term (Estrada and Kanwal (2000)). The regular term was evaluated using standard Gaussian quadrature and the singular terms were evaluated using the special Gaussian quadrature. For the hypersingular, it was used the Hadamard finite part (Ang (2014)) as follows in Eq. (13):

$$\int_{-1}^{1} \frac{f(\xi)}{(\xi-\xi_0)^2} d\xi = \int_{-1}^{1} \frac{f(\xi) - f(\xi_0) - f'(\xi_0)(\xi-\xi_0)}{(\xi-\xi_0)^2} d\xi + f'(\xi_0) \log\left(\frac{1-\xi_0}{1+\xi_0}\right) + f(\xi_0)\left(-\frac{1}{1+\xi_0} - \frac{1}{1-\xi_0}\right), \tag{13}$$

where $f(\xi)$ is a regular function. The new integral was then evaluated using standard Gaussian quadrature. This scheme was possible since Set 2 has nodes dislocated from the edges of the element. Taking the derivative of V_n^* with respect to

n_i we get:

$$\frac{\partial V_n^*}{\partial n_i} = -\frac{(\partial r/\partial n)(\partial r/\partial n_i)}{4\pi r^2}\langle\{4+2(1-\nu)[2(\partial r/\partial n)^2-1]\}+4(1-\nu)(\partial r/\partial n)^2\rangle+ \frac{(\mathbf{n}\cdot\mathbf{n}_i)}{4\pi r^2}\langle\{2+(1-\nu)[2(\partial r/\partial n)^2-1]\}+4(1-\nu)(\partial r/\partial n)^2\rangle+\frac{4(1-\nu)(\partial r/\partial n)\rho}{4\pi r}[(\partial r/\partial n)(\partial r/\partial n_i)-(\mathbf{n}\cdot\mathbf{n}_i)]. \tag{14}$$

Only the second term in Eq. (14) causes the singularity when integrating over the boundary and as $r \to 0$, so the other terms can be integrated numerically with just the standard Gaussian quadrature. Therefore, the expression to be regularized (looking back to Eq. (2)) is:

$$\int_{-1}^{1} \frac{\partial V_n^*}{\partial n_i}(\xi)\phi_i(\xi)|J(\xi)|d\xi = \int_{-1}^{1} \frac{f(\xi)}{(\xi-\xi_i)^2}d\xi. \tag{15}$$

After expanding the dependencies of $\mathbf{n}$, r and $(\partial r/\partial n)$ with respect to ξ, we can factor the hypersingular term and thus the remaining expression is the regular function $f(\xi)$. Its derivative is taken at ξ_0 and with that, Eq. (15) can be applied in Eq. (13).

Rigid body movement was employed to calculate the free term from every node from both sets and added to the respective location in $\mathbf{H}_V$ and to $\mathbf{H}_{M_i}$. This was done to ensure singularity treatment was behaving accordingly.

3.2 Domain integral

The presence of the domain integral in both Eq. (1) and Eq. (2) would deem necessary a domain discretization, which would defeat the purpose of using the Boundary Element Method. With that in mind, it was applied the radial integration according to Gao (2002). Since the purpose of this paper is the comparison between three types of methodologies with BEM, the acting body force was simplified to be uniform and constant over the entire domain. On that note, the domain integral was transformed according to the following equations (for simplicity the argument was hidden):

$$\int_\Omega w^* d\Omega = \sum_{j=1}^{N}\int_{\Gamma_j} \frac{1}{r_j}\frac{\partial r}{\partial n}\left(\frac{q_0 r_j^4(4\log(r_j)-1)}{128\pi D}\right)d\Gamma_j, \tag{16}$$

$$\int_\Omega \left(\frac{\partial w}{\partial n_i}\right)^* d\Omega = \sum_{j=1}^{N}\int_{\Gamma_j} -\frac{1}{r_j}\frac{\partial r}{\partial n}\left(\frac{\partial r}{\partial n_i}\frac{q_0 r_j^3(1+6\log(r_j))}{72\pi D}\right)d\Gamma_j, \tag{17}$$

where N is the number of boundary elements. The given integrals were evaluated numerically. The resulting vector contained the equivalent domain integral for each source point relative to the respective integral (the same source could generate a value from either from Eq. (16) or Eq. (17)).

4. RESULTS

For all scenarios, it was used $\nu = 0.3$, plate thickness $h = 10\,mm$, Young's modulus $E = 200\,GPa$ netting a flexural rigidity of $D = 18.315\,KPa.m^3$. Each case will be referred by the boundary conditions of the plate's sides as follows: **S** for simply supported, **C** for clamped and **F** for free edge. Data will be plotted starting with 10 elements per side, since lower number of elements can generate inaccurate results. Since a unitary uniform load was applied, the reference value for those cases was simply the geometry's area.

4.1 Polygonal plates

All plates in this section are squares with $L = 1\,m$. Figures 7 and 8 show the convergence of the displacement at the center (Point 0) of the plate and the total resulting force from Eq. (11) for the fully simple supported case (**SSSS**). All models converged properly to the answer, but initial response was better for the outside points model. As observed, the peak was an error of 0.005 % from the reference value. Analytical normalized answer for Fig. 7 is 0.00406235 (Timoshenko and Woinowsky-Krieger (1959)).

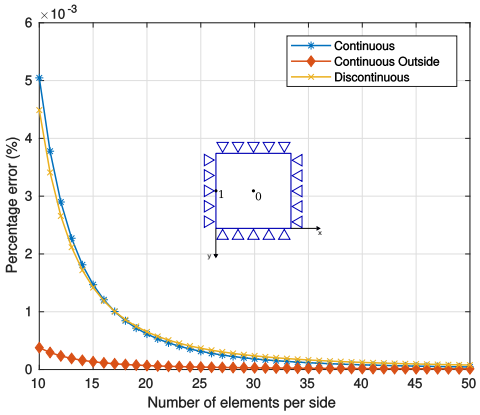

Figure 7. Convergence of w - Case **SSSS**

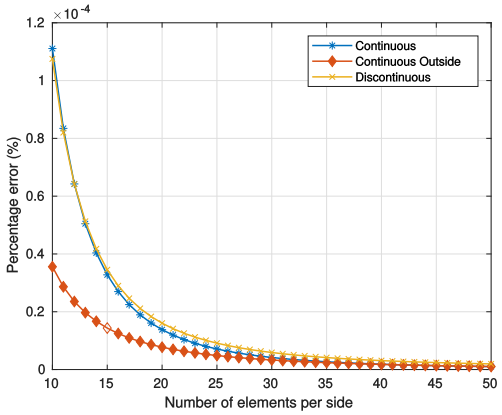

Figure 8. Convergence of the body force - Case **SSSS**

Figures 9, 10 and 11 show the convergence of the displacement at middle of the free side (Point 0), the bending moment in the normal direction and the effective shear force at the middle of the clamped edge (Point 1) for the case **SFSC**. Both discontinuous and continuous model showed quick convergence and presented virtually equal values at 50 elements per side for both displacement and bending moment. The outside points model while previously showing better results now exhibited a different behaviour, especially with more inaccuracy on the bending moment values (still as high as 12% with a total of 40 elements). Analytical normalized answer for Fig. 9 is 0.0113; for Fig. 10 is -0.119 (both from Timoshenko and Woinowsky-Krieger (1959)). FEM normalized answer for Fig. 11 is -0.696 (Katsikadelis (2014)).

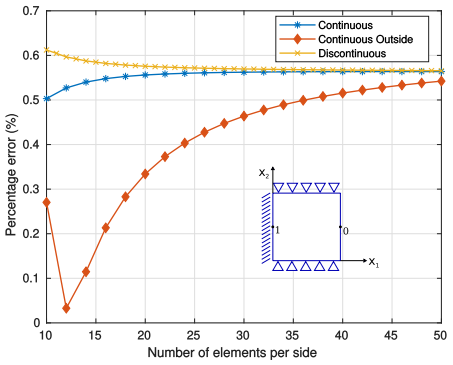

Figure 9. Convergence of w - Case **SFSC**

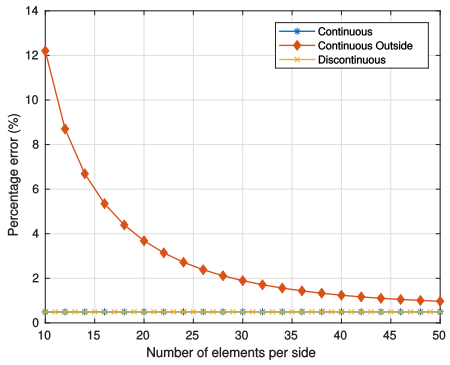

Figure 10. Convergence of M_n - Case **SFSC**

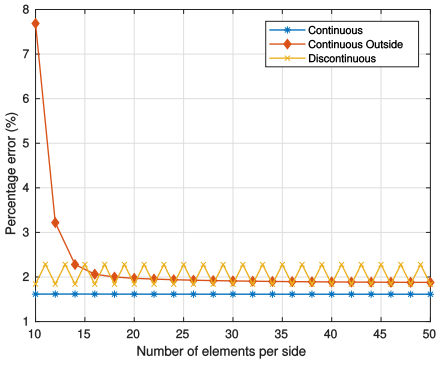

Figure 11. Convergence of V_n - Case **SFSC**

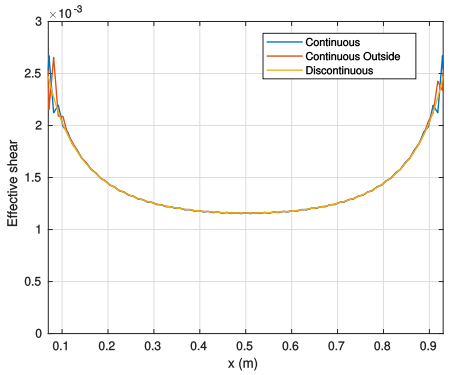

Figure 12. Distribution of V_n - Case **FFFC**

Figure 12 shows the distribution of V_n (reference value is -1.161 from Katsikadelis (2014)) across most of the clamped edge of a cantilever plate (case **FFFC**) and Fig. 13 provides a closer look at the results at the edge of the clamped side (with the extrapolation at $x = 1\,m$ for the discontinuous model). Figure 14 shows the results observed by Venturini and Paiva (1993). Since data nodes were so close to each other, they have been omitted in Fig. 12 for visibility. In theory, Case 2 (from Reissner's Theory) is the expected response to this case and all models somewhat accomplishes that across most of the boundary (despite the curvature depicted which is negligible due to scale).

As noted by Ramos and Souza (2017), the peaks showed by the continuous and the outside points models could be interpreted to happen due to the use of point collocation exactly at the corner ends of the edge, whereas the discontinuous model has nodes slightly shifted from the corner. The stress concentration at the corner is a feature of the problem as well as being a point where the shear force suddenly reaches 0, therefore it is a more accurate representation of the problem than what is displayed by the discontinuous model.

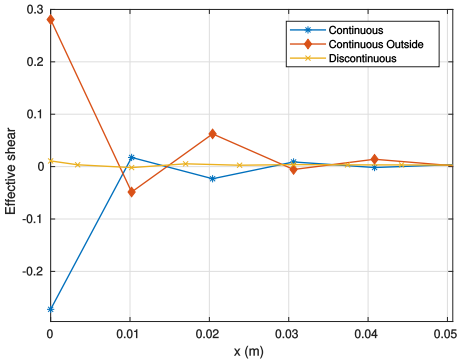

Figure 13. Detail at the edge of the clamped side

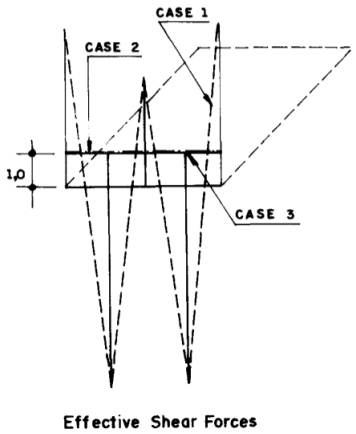

Figure 14. Distribution results according to Venturini and Paiva (1993)

As mentioned before, the equilibrium was also checked for each model in each case. As it can be seen on Fig. 15 and Fig. 16, the continuous and discontinuous models keep a magnitude of error close to zero while the outside points model presented some inconsistencies, as it is expected from the model.

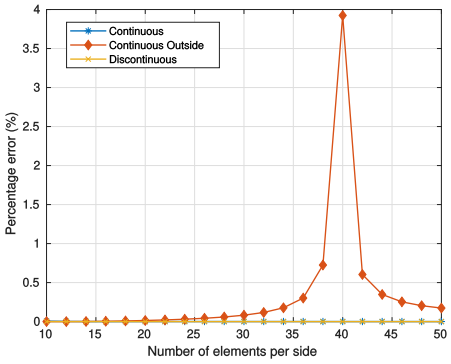

Figure 15. Convergence of the body force - Case **CFSS**

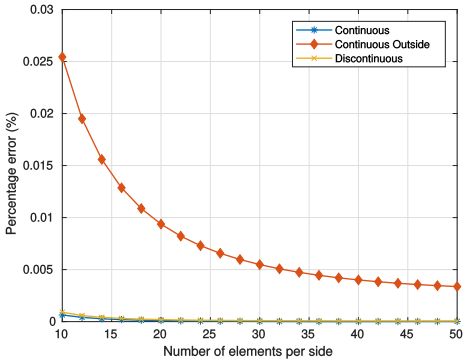

Figure 16. Convergence of the body force in case **SFSC**

Using the MATLAB® function "*rcond*", it is possible to evaluate how close to singular a matrix is. As expected, starting from 20 elements per side, all matrices **A** (from case **CFSS**) were close to singular (the function returns a value close to zero, that is, smaller than 2^{-52}). This is due to the chosen distance for point collocation, as this behaviour was seen in other cases as shown in Fig. 17: displacement error decreases but increases for the bending moment the closer to the boundary the source nodes are. Analytical normalized answer for the displacement and bending moment for Fig. 17 are 0.0012644 and -0.0513 (Timoshenko and Woinowsky-Krieger (1959)). The abscissa shows the relation between the distance used to the element size, therefore it's dimensionless.

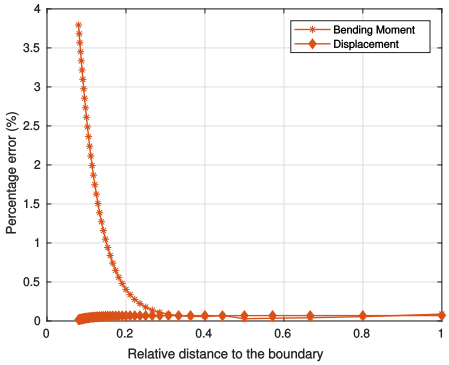

Figure 17. Convergence of displacement and bending moment for the outside points model - Case **CCCC**

4.2 Curved plates

Figure 18 and Fig. 19 show the convergence of the displacement at the center of the plates (Point 0) for a fully simple supported circular plate and for an elliptical plate ($a/b = 1.5$) clamped on all edges. The boundary mesh was evenly distributed per quadrant ("side"). It is worth noting that in both scenarios, the error was under 1% for all models (except for the outside points model on the circular plate) with just 2 elements per quadrant. Analytical normalized answer for the displacement for Fig. 18 is 0.0637019 and for Fig. 19 is 0.0278926 (both from Guminiak (2010)). The influence of the matrix conditioning impacted the results for the outside points model in both scenarios.

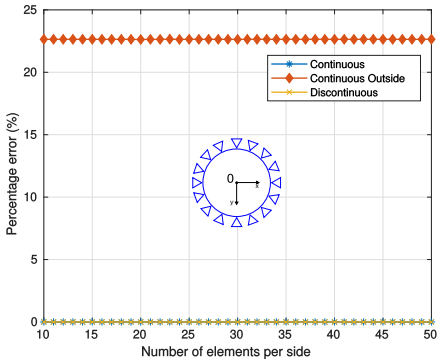

Figure 18. Convergence of w - Case **SSSS**

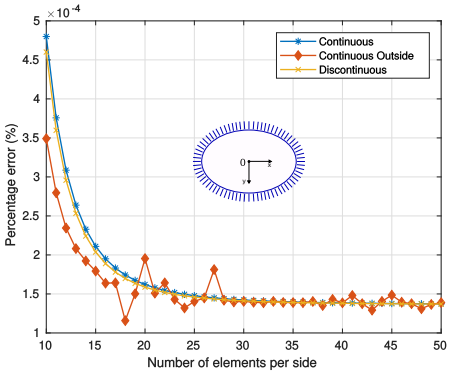

Figure 19. Convergence of w - Case **CCCC**

4.3 Extra examples

An extra example was made to further investigate the algorithm's behaviour across unusual shapes. The results for the normalized displacement at an internal point and the for the body forces for the case **CFCFC** is shown in Fig. 20 and Fig. 21. The reference value of the displacement was obtained via ABAQUS®, using 12992 elements of STRI3 type for this is the element type closest to the Kirchhoff's theory of thin plates. The normalized value encountered via FEM for the displacement at point 0 was 0.0190484.

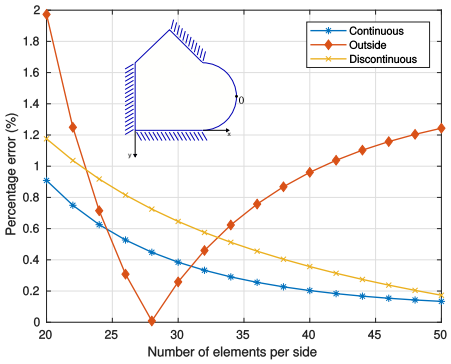

Figure 20. Convergence of w - Case **CFCFC**

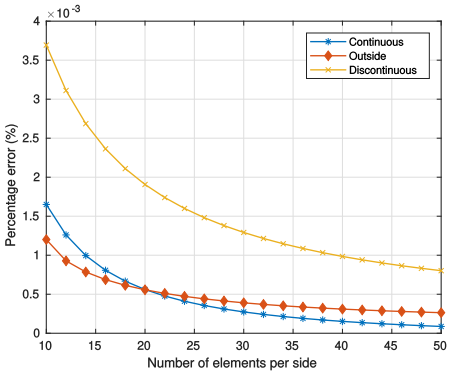

Figure 21. Convergence of the body force - Case **CFCFC**

Despite the outside points model eventually reaching an error lower than the other two models, it proceeded to diverge from the reference value, thus remaining unreliable. Both continuous and discontinuous models converge properly to the answer, with the first being more precise than the latter.

5. CONCLUSIONS

A methodology for comparison of different boundary element methods was created. For each model, it was discussed how the algorithm would work taking in consideration treatment of singularities, node allocation, continuity of variables and transforming the domain integral (regarding the body force) into a boundary integral, making it a fully boundary methodology.

During the creation of the algorithm for the outside points model, several problems were faced with the placement of the nodes. Eventually, one strategy was devised in which the values of V_n and M_n greatly improved overall. One interesting remark is that the values of displacement would always have a low (or very low) percentage error no matter the distance chosen (within reason). However, the same can't be said about the other variables.

As it can be observed from the figures presented, the continuous model converged to the answer in all of the scenarios, despite fluctuations. The outside points model presented inconsistencies due to point collocation proximity, which sometimes led to a badly scaled matrix (as it was the case for the curved plates or highly populated meshes).

Considering the inconsistency of point collocation from the outside points model and the lack of representation of corners in the discontinuous model (despite the some good results), the continuous model has shown to be more reliable out of the three models presented when analyzing isotropic Kirchhoff plates of any given shape and/or boundary conditions.

6. REFERENCES

Ang, W.T., 2014. *Hypersingular integral equations in fracture analysis*. Woodhead Publishing.

Brebbia, C.A. and Dominguez, J., 1991. *Boundary Elements: An introductory course*. WIT Press, 2nd edition.

Estrada, R. and Kanwal, R.P., 2000. *Singular Integral Equations*. Birkhäser.

Gao, X.W., 2002. "The radial integration method for evaluation of domain integrals with boundary-only discretization". *Engineering Analysis with Boundary Elements*, Vol. 26, pp. 905–916. doi:10.1016/S0955-7997(02)00039-5.

Guminiak, M., 2010. "Application of simplified curved boundary elements to the plate analysis - part two". *Scientific Research of the Institute of Mathematics and Computer Science*, Vol. 9, pp. 73–81.

Hartmann, F. and Zotemantel, R., 1986. "The direct boundary element method in plate bending". *International Journal for Numerical Methods in Engineering*, Vol. 23, No. 11, pp. 2049–2069. doi:10.1002/nme.1620231106.

Katsikadelis, J.T., 2014. *Boundary Element Method for Plate Analysis*. Elsevier Inc.

Ramos, C. and Souza, C., 2017. "Potential and elastostatic analysis in non homogeneous two-dimensional domains using the boundary element method". In *Proceedings of the XXXVIII Iberian Latin-American Congress on Computational Methods in Engineering*. doi:10.20906/CPS/CILAMCE2017-1265.

Stern, M., 1979. "A general boundary integral formulation for the numerical solution of plate bending problems". *International Journal of Solids and Structures*, Vol. 15, No. 10, pp. 769 – 782. ISSN 0020-7683. doi: https://doi.org/10.1016/0020-7683(79)90003-9.

Tanaka, M. and Bercin, A., 1998. "Static bending analysis of stiffened plates using the boundary element method". *Engineering Analysis with Boundary Elements*, Vol. 21, pp. 147–154. doi:10.1016/S0955-7997(98)00002-2.

Timoshenko, S. and Woinowsky-Krieger, S., 1959. *Theory of Plates and Shells*. McGraw Hill, New York, 2nd edition.

Venturini, W. and Paiva, J., 1993. "Boundary element for plate bending analysis". *Engineering Analysis with Boundary Elements*, Vol. 11. doi:10.1016/0955-7997(93)90072-S.

7. RESPONSIBILITY NOTICE

The authors are the only responsible for the printed material included in this paper.